PROCEEDINGS OF SCIENCE

X-ray jets from the X-ray binary Cir X-1

P. Soleri*[a], S. Heinz[b], R. Fender[c,a], R. Wijnands[a], V. Tudose[a,d,e], D. Altamirano[a], P.G. Jonker[f,g], M. van der Klis[a], L. Kuiper[f], C. Kaiser[c], P. Casella[a]

[a] *Astronomical Institute "A. Pannekoek", University of Amsterdam, Kruislaan 403, NL-1098 SJ, Amsterdam, The Netherlands*

[b] *Astronomy Department, University of Wisconsin-Madison, 475 N. Charter St. Madison, WI 53705, US*

[c] *School of Physics and Astronomy, University of Southampton, Highfield, Southampton SO17 1BJ*

[d] *Astronomical Institute of the Romanian Academy, Cutitul de Argint 5, RO-040557 Bucharest, Romania*

[e] *Research Center for Atomic Physics and Astrophysics, Atomistilor 405, RO-077125 Bucharest, Romania*

[f] *SRON, Netherlands Institute for Space Research, Sorbonnelaan 2, 3584 CA, Utrecht, the Netherlands*

[g] *Harvard-Smithsonian Center for Astrophysics, Cambridge, MA 02138, US*

Email: p.soleri@uva.nl, heinzs@astro.wisc.edu, rpf@phys.soton.ac.uk, R.A.D.Wijnands@uva.nl, V.M.Tudose@uva.nl, d.altamirano@uva.nl, p.jonker@sron.nl, michiel@science.uva.nl, L.M.Kuiper@sron.nl, crk@astro.soton.ac.uk, P.Casella@uva.nl

We present the results of the analysis of two *Chandra* observations of Circinus X-1 performed in 2007, for a total exposure time of ∼50 ks. The source was observed with the High Resolution Camera during a long X-ray low-flux state of the source. Cir X-1 is an accreting neutron-star binary system that exhibits ultra-relativistic arcsec-scale radio jets and an extended arcmin-scale radio nebula. Furthermore, a recent paper has shown an X-ray excess on arcmin-scale prominent on the side of the receding radio jet. In our images we clearly detect X-ray structures both on the side of the receding and the approaching radio jet. The X-ray emission is consistent with being from synchrotron origin. Our detection is consistent with neutron-star binaries being as efficient as black-hole binaries in producing X-ray outflows, despite their shallower gravitational potential

VII Microquasar Workshop: Microquasars and Beyond
September 1-5 2008
Foca, Izmir, Turkey

*Speaker.

PoS(MQW7)048

1. Introduction

Cir X-1 was discovered in 1971 [18] and has been showing fares with a period of 16.55 days, observed first in the X-ray band [16] and then in the infrared ([8]; [9]), radio [12] and optical bands [19]: this fact is interpreted as enhanced accretion close to the periastron passage of a highly eccentric binary orbit ($e \sim 0.8$, [20], [21]). Beyond variability at the 16.55 day orbital period the source shows dramatic evolution of its X-ray luminosity, spectra and timing properties on timescales from milliseconds [23] to decades [22], alternating bright flares and periods of very low X-ray flux. The evidence that the system harbours a neutron star comes from the detection of type-I X-ray bursts [25] and twin kHz QPOs in the X-ray power density spectra [2]. The source is located in the Galactic plane at a distance that has been reported to lie in the range 4-12 kpc ([13], [14]).

Cir X-1 is one of the most radio-loud neutron star X-ray binary ([28], [12]), showing extended-radio structures both at arcmin and arcsec scale. The arcmin-scale structure has been extensively studied ([24], [26]): the source shows two radio jets (south-east and north-west direction) embedded in a large scale, diffuse radio nebula. There is general agreement that this nebula is the result of the radio lobe inflated by the jets over several hundred-thousand years. Arcmin-scale jets are curved which might be due to an interaction with the interstellar medium (ISM) or a precessing jet. On arcsec scale, the source shows a one-sided highly-variable jet [6], the most relativistic one detected so far within our Galaxy [7], with a bulk Lorentz factor ≥ 10.

On 2005 June 2nd *Chandra* observed Cir X-1 with the High Energy Transmission Gratings (HETGS) for 50 ks during one of its long-term X-ray low-flux states (an example of X-ray light curve with long periods of low flux is reported in Figure 1), detecting an arcmin-scale X-ray structure prominent on the side of the receding radio jet [11]. While for black hole candidates extended X-ray jets have already been detected in a number of sources (e.g. XTE J1550-564 [4]; 4U 1755-33 [1]; H1743-322 [5]), this is the first detection of X-ray structures in a secure neutron star system, showing that neutron stars can be as efficient as black holes in producing X-ray outflows.
Here we present recent *Chandra* observations of Cir X-1 where we clearly detect an extended X-ray structure both on the side of the approaching and the receding radio jet, confirming and extending the detection reported in [11].

2. Observation and data analysis

Cir X-1 was observed with the High Resolution Camera (HRC) onboard the *Chandra* X-ray Observatory on 2007 April 21st (43 ks, observation A) and on 2007 May 16th (7 ks, observation B), during an exceptionally long interval of very low X-ray flux that occurred from $\sim$ 2007 February until $\sim$ 2007 August (see Figure 1). For more details on the data analysis, see Soleri et al. (2008), submitted to MNRAS.

2.1 X-ray jets

Images from observations A and B are reported in Figure 2. A visual inspection of the images clearly reveals the presence of an extended X-ray structure around the source up to $\sim$arcmin scale, visible in the South-East and in the North-West quadrant (i.e. aligned with the South-East - North-West direction), consistent both with the results recently reported in [11] and with the alignment of

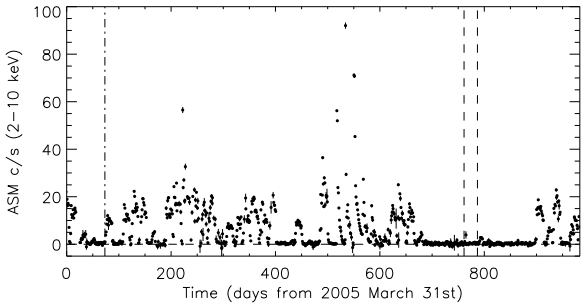

Figure 1: RXTE/ASM daily-average light curve from 2005 March 31 to 2007 November 29. The vertical dashed lines correspond to two *Chandra*/HRC-I observations, the vertical dashed-dotted line corresponds to the HETGS observation analysed in [11].

the arcmin-scale jet ([24], [26]); this issue will be discussed in §2.2.

The extended emission is detected both in obs. A and B and the two images (note the different exposure in the two observations), at a visual inspection, are consistent: the X-ray emission around the central source, in both of them, elongates along the same axis and furthermore, it presents similar structures in the North-West quadrant and a similar spike-like structure in the northern quadrant (although there are differences especially in the South-East quadrant, due to different sensitivity limits).

Since the two images are consistent, we can merge them to have an image with a higher equivalent exposure, using the standard *Ciao 4.0* analysis tools. We adaptively smoothed the image obtained from the merging with an average significance of 8.3σ per smoothing length and we applied contour levels. The resulting image is plotted in Figure 2 (panel (c)), where a diffuse X-ray emission elongated along the South-East - North-West direction is evident, extending up to $\sim$1 arcmin from the point source. Other structures might look real from an analysis of this image (e.g a circular excess in the South-West quadrant) but they will not be discussed since an inspection of the residuals obtained after fitting the point spread function (PSF) suggests that they are noise features (see next part of this paragraph).

Figure 3 shows two profile cuts (for obs. A), one extracted on a region aligned with the X-ray excess and one along the perpendicular axis, showing an excess along the South-East - North-West axis and supporting the evidence that there is an X-ray extended structure aligned with a privileged direction.

From Figure 2 (panels (a), (b) and (c)) and Figure 3 the presence of an extended X-ray structure around the central source is evident but to make our detection more robust, an analysis of the PSF is needed. We simulated a monochromatic PSF at 1 keV (we expect the X-ray excess emission to peak at this energy [11]) using *ChaRT*, considering the same number of counts as detected from the source and we projected it in the detector plane using the *Marx* ray tracing. Since the PSF wings depend on the position on the detector, for the PSF analysis we used only the obs. A: even if the image from the merging has a higher equivalent exposure, the PSF extracted from that image might contain artefacts (the source position on the detector is not the same for obs. A and B) that we want to avoid. For the PSF analysis, the *Sherpa 3.4* tools have been used.

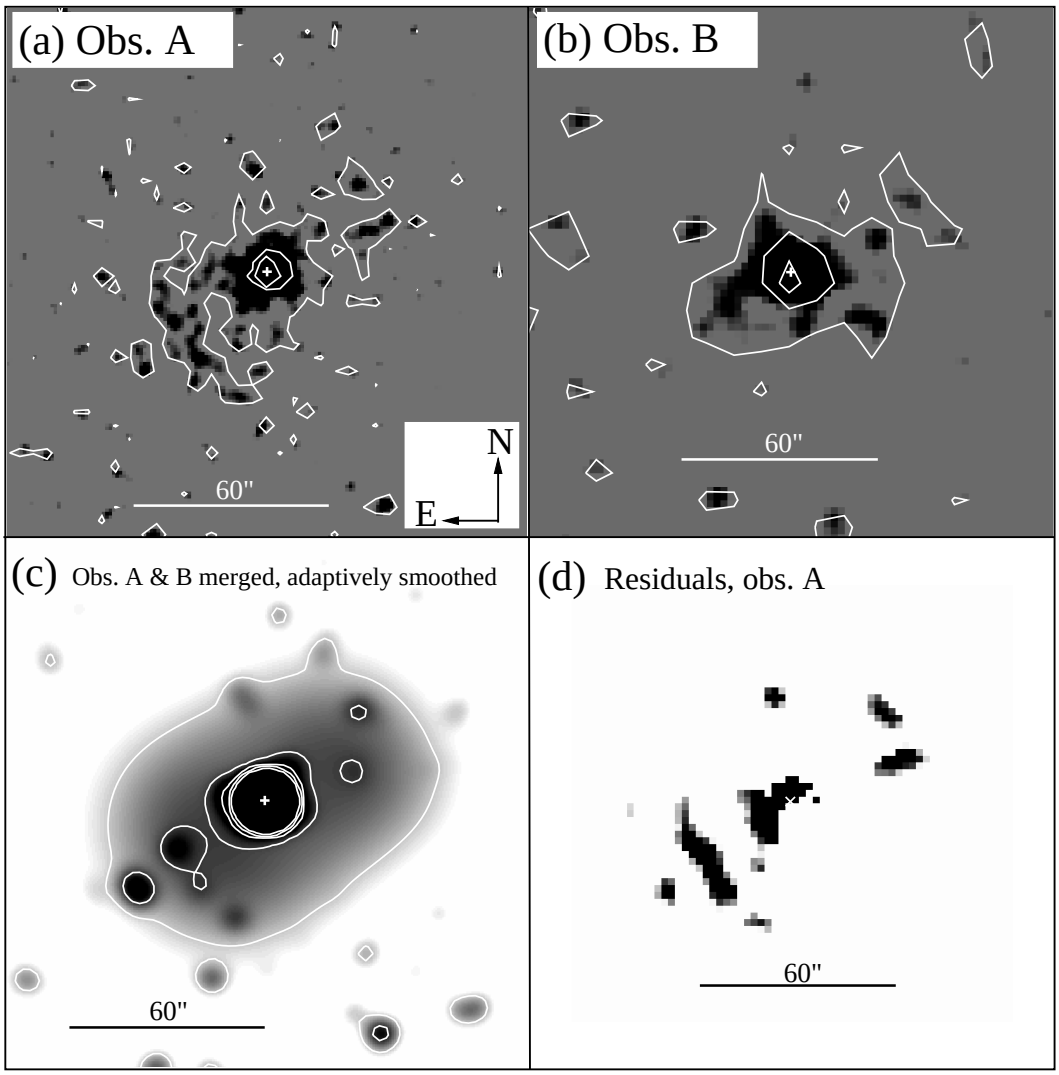

Figure 2: (a) *top left:* HRC-I image of obs. A. (b) *top right:* HRC-I image of obs. B. (c) *bottom left:* image of the merger of obs. A and B, adaptively smoothed. (d) *bottom right:* image of the residuals obtained after fitting the source image (obs. A) with a gaussian function and a constant using the PSF image as the convolution kernel. In all the panels we marked the source location with a cross.

In Figure 2 (panel (d)) we show the image of the residuals obtained after fitting the source image with a gaussian function and a constant using the PSF image as the convolution kernel. The presence of an extended X-ray structure aligned with the South-East - North-West axis is evident, at a distance from the central source between ~ 25" and ~ 50" (the lower limit is inferred by inspecting both the residuals image and the radial profile image in Figure 3). The X-ray excess on the side of the receding radio-jet (North-West quadrant, hereafter "receding X-ray jet") lies at position angle (PA, measured counterclockwise from due North from the point source) intervals 286°-295° and 307°-324°. A knot appears also at PA $\sim 10°$ and its identification will be discussed in the next sub-section. On the side of the approaching radio jet (South - East quadrant) we see one main X-ray blob in a PA interval 88°-152° (elongated along a North-East - South-West direction, hereafter

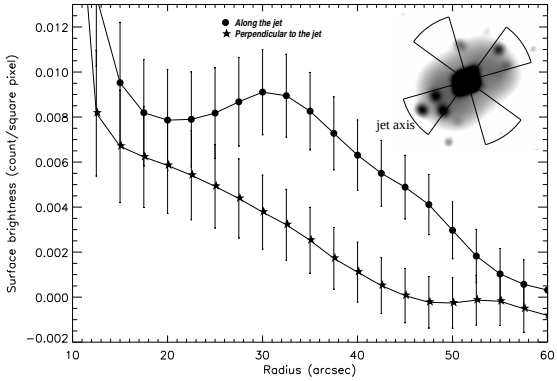

Figure 3: Radial surface-brightness profile extracted, for obs. A, across the jet (circles) and across a region perpendicular to the jet (stars). The extraction regions are shown in the inset and correspond to the following PAs (see definition in the text): X-ray excess 106°-144° and 286°-324°; axis perpendicular to the X-ray excess 16°-54° and 196°-234°.

"approaching X-ray jet"), at a distance from the point source between 28" and 38". Other minor blobs appear in the residuals image: all of them are located in the South - East quadrant and are consistent with being knots of the approaching X-ray jet.

2.2 Comparison with previously detected X-ray extended structure and the radio jet

The radio nebula and the relativistic radio-jets of Cir X-1 have been investigated during multiple epochs of radio observations, both on arcmin and arcsec scale ([24], [6], [7], [26], [27]). From those papers, we estimate the corresponding PAs: $310^\circ \pm 15^\circ$ for the arcmin-scale jets detected in [26] and $320^\circ \pm 4^\circ$ for the ultrarelativistic jets detected on arcsec scale in [7]. All these angles are consistent with the PAs of the X-ray jets in our HRC-I observations and fall between the two X-ray filaments detected in [11] in the HETGS image.
Figure 4 shows an overlay of the residuals image (the same as Figure 2 panel (d), grey scale), the X-ray contours from Figure 2 panel (c) and the jet emission from Figure 1 of [11]. Also shown are the radio contours from Figure 3 of [26] and the limits on the PA for the arcsec-scale jet [7]. The X-ray jets detected in the HRC-I images are broadly consistent with the X-ray excess of [11]. Besides the X-ray knot that we detected at PA 10°, the consistency between the X-ray and the radio jets is clear on both sides (approaching and receding): what we see in the HRC-I images appears as the X-ray counterpart of the radio jets from Cir X-1.

3. Discussion and conclusions

The analysis of our two HRC-I observations of Cir X-1 clearly showed X-ray jets both on the side of the receding and the approaching radio jet, consistent with being the X-ray counterpart of the arcmin-scale radio jets [26]. Two possible alternative explanations have been suggested [11] for the origin of the X-ray excess: synchrotron emission and thermal bremsstrahlung. We now investigate whether these two mechanisms can still explain the X-ray jets as observed by HRC-I.

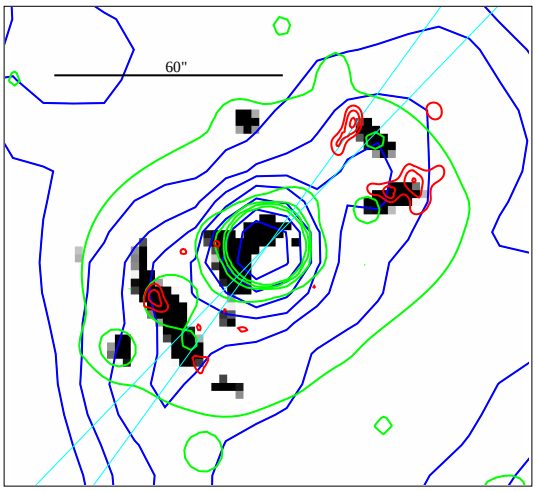

Figure 4: Radio-X-ray overlay. Grey scales: X-ray residuals image (Fig. 2 (d)); green contours: adaptively smoothed image of obs. A & B merged (Fig. 2 (c)); red contours: adaptively smoothed, normalized, PSF subtracted image (from [11]); dark blue contours: 1.4 GHz surface brightness (adapted from [26], levels increase by $\sqrt{2}$ between contours, outermost contour: 11.2 mJy/beam); light blue lines: estimated allowed range of PAs from high-resolution radio observations of approaching radio-jet [7]. The crossing of these two lines identify the source position.

Synchrotron emission: HRC-I does not have the energy resolution necessary to allow for spectral fitting, instead we calculate the jet flux with *webPIMMS*[1] using, as input spectrum, the absorbed power law fitted in [11] ($\Gamma = 3.0^{+2.6}_{-1.5}$, $N_H = 5.9 \times 10^{22}$ cm^{-2}) and the average count rate extracted, for obs. A, in the region corresponding to the main knot of the approaching jet, using *Ciao 4.0*. This gives an un-absorbed flux $F_{2-10keV} = 7.4 \times 10^{-13}$ erg cm^{-2} s^{-1}, corresponding to an X-ray luminosity $L_{2-10keV} = 5.4 \times 10^{33}$ erg s$^{-1} D^2_{7.8}$ (throughout the paper we adopt a distance from the source $D = 7.8$ kpc, the same adopted in [11], to make comparisons easier). The used photon index Γ is broadly consistent with the emission being of synchrotron origin ($\Gamma_{syn} \sim 1.5$); assuming a source volume V, a specific luminosity L_ν and a spectrum of the form $L_\nu \propto \nu^\alpha$, ($\alpha = 1 - \Gamma$), we can estimate the minimum energy associated with the source [17]. The morphology of the jet suggests that we are observing the surface of a conical volume where the emission takes place. Considering the jet length to be roughly $l_{jet} \approx 1.6$ pc $D_{7.8}/sin\,i$ (where i is the angle with the line of sight) and a half-opening angle $\beta \approx 19.3^\circ$ the volume of the emitting cone is $V_{jet} = 9.7 \times 10^{55}cm^3 D^3_{7.8}/sin\,i$, assuming equal emitting volumes both on the receding and on the approaching side. Under these assumptions the minimum jet energy is $E_{min} \gtrsim 6 \times 10^{44}$ erg. Again following [17], we can calculate the magnetic field B_{min} associated to E_{min}, the Lorentz factor γ of the energetic electrons emitting by synchrotron and their gyro-radius r_g: $B_{min} = 8.2\mu$G, $\gamma = 2.3 \times 10^8$ and $r_g = 1.6 \times 10^{-2}$ pc. The energy of these electrons is $E_e = 1.2 \times 10^{14}$ eV and their energy loss rate is $R \sim 2300$ eV/s: considering that we have no evidence for re-acceleration taking place, the lifetime t_{syn} of these electrons is $t_{syn} \approx 1600$ yr. Following [26], we assume that the jets are injected mainly during the flare states (duty cycle $\sim$6%): the resulting minimum jet power is $W_{syn} \gtrsim 2 \times 10^{35}$ erg/s.

Thermal bremsstrahlung: in this case the X-rays would originate from the shock driven

[1] http://heasarc.nasa.gov/Tools/w3pimms.html

into the ISM by the propagation of the jets. Here we use a model developed for extragalactic jet sources ([3], [15] and [10]). We assume the temperature of the thermal gas to be $k_B T_{shock} = 2.2$ keV ($k_B T_{shock} = 2.2^{+7.0}_{-1.1}$ keV and $N_H = 5.4 \times 10^{22}$ cm^{-2} are obtained in [11] fitting the jet spectrum with an absorbed thermal model), the electron density to be $n_e \approx 10$ cm^{-3} (as used in [11]; since the temperature $T_{shock} = 25.5$ MK we assume an ionization fraction x=1: all the hydrogen is ionized) and the length of the shock region (considering both receding and approaching side) $L_{shock} \approx 2.27$ pc. Such length and the used density give an emitting gas mass (for each side of the jet) of 0.02-0.3 $M_\odot D_{7.8}^{5/2}/sin i$: uncertainties are due to different possible measures of the thickness of the shock region. Following [15] and balancing the interior pressure exerted by the jets and the ram pressure of the shocked ISM, the jet lifetime is $t_{th} = \frac{3}{5}\frac{L}{v_{sp}} \approx 1700$ yr (v_{sp} is the velocity of the shock-compressed particles, obtained from the shock temperature $k_B T_{shock} = 2.2$ keV) and the jet power is $W_{th} \approx 6 \times 10^{37}$ erg/s.

Discussion: In the synchrotron case the jet lifetime t_{syn} is smaller than the time expected for the jet to inflate the large-scale radio lobe ($10^4 - 10^5$ yr, [26]) and this suggests that the X-ray emission could come from the jet itself rather than from the inflated radio nebula. Furthermore, the gyro-radius of the electrons responsible for the X-rays is smaller than the size of the jet ($r_g < l_{jet}$) and this implies that those electrons can be confined in the jet region. Our jet power value is consistent with the estimate reported in [26] ($W_{jet,Tudose} \sim 10^{35}$ erg/s, which however could be up to two order of magnitude higher) and one order of magnitude smaller than the jet power calculated in [11] ($W_{syn,Heinz} \gtrsim 5 \times 10^{36}$ erg/s). The magnetic field associated to the emitting electrons is again consistent with the value reported in [26] ($B_{min,Tudose} = 6.3\mu$G), making W_{syn} a robust estimate of the jet power, sufficient to inflate the radio nebula. W_{syn} is $\gtrsim 0.1\%$ of the Eddington luminosity ($L_{Edd} = 1.8 \times 10^{38}$ erg/s) for a $1.4 M_\odot$ neutron star: Cir X-1 is only slightly super-Eddington and this would imply a jet-production efficiency $\eta \gtrsim 0.01\%$, consistent with the previous estimate, $\eta \gtrsim 0.5$ % [11].

In the thermal bremsstrahlung case we calculated a jet power $W_{th} \approx 6 \times 10^{37}$ erg/s, two orders of magnitude larger than W_{syn} and possibly not consistent with the values estimated in [11] ($W_{th,Heinz} = 5 \times 10^{36}$ erg/s). Furthermore, W_{th} is a significant fraction ($\sim 33\%$) of the Eddington luminosity ($L_{Edd} = 1.8 \times 10^{38}$ erg/s) for a $1.4 M_\odot$ neutron star and this would be an extremely high jet-production efficiency $\eta \approx 3\%$, even for an accreting black hole. Considering this high efficiency and a typical mass accretion rate $\dot{M} = 10^{18}$ g s^{-1} the time required to inflate the jets would be $\sim$88 Myr, much bigger than $t_{th} \approx 1700$ yr, suggesting that the emission is not coming from the jet itself. Therefore thermal bremsstrahlung appears as an unlikely emission mechanism (especially compared to the synchrotron case) for the X-ray jets.

References

[1] Angelini, L., White, N. E., 2003, ApJL, 586, L71

[2] Boutloukos, S., van der Klis, M., Altamirano, D., Klein-Wolt, M, Wijnands, R., Jonker, P. G., Fender, R. P., 2006, ApJ, 653, 1435

[3] Castor, J., McCray, R., Weaver, R., 1975, ApJL, 200, L107

[4] Corbel, S., Fender, R. P., Tzioumis, A. K., Tomsick, J. A., Orosz, J. A., Miller, J. M., Wijnands, R., Kaaret, P., 2002, Science, 298. 196

[5] Corbel, S., Kaaret, P., Fender, R. P., Tzioumis, A. K., Tomsick, J. A., Orosz, J. A., 2005, ApJ, 632, 504

[6] Fender, R., Spencer, R., Tzioumis, T., Wu, K., van der Klis, M., van Paradijs, J., Johnston, H., 1998, ApJL, 506, L121

[7] Fender, R., Wu, K., Johnston, H., Tzioumis, T., Jonker, P., Spencer, R., van der Klis M., 2004, Nat, 427, 222

[8] Glass, I. S., 1978, MNRAS, 183, 335

[9] Glass, I. S., 1994, MNRAS, 268,742

[10] Heinz, S., Reynolds, C. S., Begelman, M. C., 1998, ApJ, 501, 126

[11] Heinz, S., Schulz, N. S., Brandt, W. N., Galloway, D. K., 2007, ApJL, 663, L93

[12] Haynes, R. F., Jauncey, D. L., Murdin, P. G., Goss, W. M., Longmore, A. J., Simons, L. W. J., Milne, D. K., Skellern, D. J., 1978, MNRAS, 185, 661

[13] Jonker, P. G. & Nelemans, G., 2004, MNRAS, 354, 355

[14] Jonker, P. G., Nelemans, G., Bassa, C. G., 2007, MNRAS, 374, 999

[15] Kaiser, C. R., Alexander, P., 1997, MNRAS, 286, 215

[16] Kaluzienski, L. J., Holt, S. S., Boldt, E. A., Serlemitsos, P. J., 1976, ApJL, 208, L71

[17] Longair, M. S., 1994, High Energy Astrophysics. Cambridge Univ. Press, Cambridge

[18] Margon, B., Lampton, M., Bowyer, S., Cruddace, R., 1971, ApJL, 169, L23

[19] Moneti, A., 1992, A&A, 260, L7

[20] Murdin, P, Jauncey, D. L., Lerche, I., Nicolson, G. D., Kaluzienski, L. J., Holt, S. S., Haynes, R. F., 1980, A&A, 87, 292

[21] Nicolson, G. D., Glass, I. S., Feast, M. W., 1980, MNRAS, 191, 293

[22] Parkinson, P. M. S., Tournear, D. M., Bloom, E. D., Focke, W. B., Reilly, K. T., Wood, K. S. Ray, P. S., Wolff, M. T., Scargle, J. D., 2003, ApJ, 595, 333

[23] Shirey, R. E., Bradt, H. V., Levine, A. M., 1999, ApJ, 517, 472

[24] Stewart, R. T., Caswell, J. L., Haynes, R. F., Nelson, G. J., 1993, MNRAS, 261, 593

[25] Tennant, A. F., Fabian, A. C., Shafer, R. A., 1986, MNRAS, 221, 27P

[26] Tudose, V., Fender, R., Kaiser, C., Tzioumis, A., van der Klis, M., Spencer R., 2006, MNRAS, 372, 417

[27] Tudose, V., Fender, R. P., Tzioumis, A. K., Spencer, R. E., van der Klis, M., 2008, arXiv0807.5108

[28] Whelan, J. A. J., Mayo, S. K., Wickramasinghe, D. T. Murdin, P. G., Peterson, B. A., Hawarden, T. G., Longmore, A. J., Haynes, R. F., Goss, W. M., Simons, L. W., Caswell, J. L., Little, A. G., McAdam, W. B., 1977, MNRAS, 181, 259